JOURNAL OF MATERIALS SCIENCE 23 (1988) 958–967

The mechanical and electrical properties of ZrO_2–Naβ''-Al_2O_3 composites

YIN SHENG, PARTHO SARKAR, PATRICK S. NICHOLSON
Ceramic Engineering Research Group, Department of Materials Science and Engineering, McMaster University, Hamilton, Ontario, Canada

ZrO_2–Naβ''-Al_2O_3 composites were prepared by a conventional method using two different powder routes and different milling liquids. The retained tetragonal-phase ZrO_2 was 85 to 90% for composites with 2.4 to 15 vol% ZrO_2. The fracture toughness (K_{Ic}) and strength increased with increasing ZrO_2 content. At 20 vol% ZrO_2, K_{Ic} and bend strength were 4.35 MPa $m^{1/2}$ and 390 MPa, respectively. Stress-induced transformation toughening is the predominant toughening mechanism. Dispersion toughening also contributes to the increase of K_{Ic}. Surface strengthening was found to be an effective strengthening method for low ZrO_2 levels. The critical tetragonal ZrO_2 grain size was found to increase from 0.86 to 1.02 μm as the ZrO_2 content increased from 2.5 to 15 vol%. A detailed study of the ionic conductivity of the 15 vol% ZrO_2 dispersed sample was conducted by an a.c. technique between $-124°$ C and $\sim 300°$ C. The bulk and total conductivities were calculated via complex-plane analysis. The total (grain and grain-boundary) ionic specific resistivity was $\sim 9\,\Omega$ cm at 300° C. The activation enthalpies of the bulk and total conductivity processes were 0.30 and 0.32 eV, respectively.

1. Introduction

The phase transformation of constrained tetragonal to monoclinic ZrO_2 can be induced by stress and the expansion involved leads to an increased fracture toughness (K_{Ic}) of the restraining matrix. This concept of ZrO_2 transformation toughening has been applied to polycrystalline β/β''-alumina ceramics with ZrO_2 dispersions [1–6]. The addition of ZrO_2 to Naβ''-Al_2O_3 substantially improves both fracture toughness and strength without compromising the superionic's electrical properties. Naβ''-Al_2O_3 is a solid electrolyte used as a membrane material in the Na–S battery. This solid electrolyte degrades above a critical current density, i_{cr}, which is related to its fracture toughness (K_{Ic}) [7, 8]. Consequently an improvement of K_{Ic} should lead to increased i_{cr} and longer battery life. Tough and strong Naβ''-Al_2O_3 is also a potential precursor material for H_3O^+ β/β''-alumina, an electrolyte of interest for the medium-temperature electrolysis of steam and H_2–O_2 fuel cells. Polycrystalline H_3O^+ β''/β-Al_2O_3 has been developed and used to electrolyse steam. The material is based on a mixed alkali K/Naβ''/β-Al_2O_3 precursor which is ion-exchanged in two stages to produce H_3O^+ β''/β-Al_2O_3. The precursor ceramic has high strength and allows the ceramic to survive the rigours of the initial ion exchange in potassium/sodium chloride or nitrate melts [9].

The present paper describes a conventional method for producing strong and tough ZrO_2–Naβ''-Al_2O_3 composite materials and defines their mechanical properties.

This paper also contains the first detailed study of the ionic conductivity of a ZrO_2–Naβ''-Al_2O_3 composite. Green and Metcalf [5] studied the ionic conductivity of ZrO_2–Naβ''-Al_2O_3 composites by an a.c. technique between 250 and 350° C in the frequency range 100 Hz to 100 kHz. At these temperatures, 100 kHz is not sufficiently high to resolve the grain and grain-boundary contributions to the ionic conductivity, so the total conductivity value was reported. Lange *et al.* [1] studied the ionic conductivity of the composites at a fixed a.c. frequency (1 kHz) between room temperature and 300° C. Fixed-frequency measurements give no indication of the total and grain (bulk) conductivity. Such conductivity results are only satisfactory for internal comparison. The present paper reports studies of the ionic conductivity between $-124°$ C and $\sim 300°$ C using a frequency range from 5 Hz to 13 MHz.

2. Experimental procedure

The composition of Naβ''-Al_2O_3 chosen was $Na_{2.0}Mg_{0.67}Al_{10.33}O_{17}$. Two routes were investigated to produce the ZrO_2–Naβ''-Al_2O_3 composite powders. In Route I, powders of Na_2CO_3, MgO and α-Al_2O_3 (Alcoa A16SG) were milled in ethanol for 48 h, dried and calcined for 5 h at 1000° C to give Naβ''-Al_2O_3 powder. After removing large agglomerates by sedimentation in water, ZrO_2–4.5 wt% Y_2O_3 (Zircar Inc. ZYP 4.5 i of %) and the calcined Naβ''-Al_2O_3 powders were milled together in ethanol for 24 h. In Route II, the fine ZrO_2 powder, Na_2CO_3, MgO and Al_2O_3 were milled in ethanol for 48 h, dried and calcined at 1000° C. Four milling liquids (ethanol, acetone, methyl alcohol and butanol) and five ZrO_2 contents

0022–2461/88 $03.00 + .12

TABLE I Effect of milling liquid on structure and properties of ZrO_2–Naβ''-Al_2O_3 composites (Powder Route II)

Milling liquid	Density (% theoretical)	Bend strength (MPa)	K_{Ic} (MPa $m^{1/2}$)	$f(\beta)$	m(%)	Grain size (μm)	
						Naβ''-Al_2O_3	ZrO_2
Acetone	97.4 to 97.7	322 ± 21	3.1 to 3.6	0.08 to 0.10	11 to 17	0.79	0.71
Methyl alcohol	97.1 to 97.7	311 ± 28	3.0 to 3.5	0.06 to 0.08	14 to 18	1.04	0.79
Ethanol	97.3 to 97.8	328 ± 29	3.1 to 3.6	0.03 to 0.05	12 to 16	0.81	0.68
Butanol	96.4 to 96.7	238 ± 37	–	0.09 to 0.12	40 to 46	1.10	0.83

(2.5, 5, 10, 15 and 20 vol %) were investigated. The sieved composite powder prepared by the two routes was uniaxially pressed, isostatically pressed at 35 000 p.s.i. (241 MPa) and sintered at 1620° C for 5 to 10 min in an Al_2O_3 crucible containing a bed of Naβ''-Al_2O_3 powder. A fast heating rate was necessary to achieve a high sintered density for the Naβ''-Al_2O_3 and the ZrO_2–Naβ''-Al_2O_3 composites. A schedule of 25 to 1620° C in 20 min yielded the maximum sintered densities. According to the $NaAlO_2$–Al_2O_3 phase diagram [10], Naβ-Al_2O_3 and $NaAlO_2$ form a binary eutectic liquid at 1585° C. This liquid is transient and promotes the densification of the Naβ''-Al_2O_3 and ZrO_2–Naβ''-Al_2O_3 composites.

The phases in the sintered specimens were determined by X-ray diffraction analysis. The relative amounts of Naβ- and Naβ''-Al_2O_3 were qualitatively assessed using the normalized index, $f(\beta)$. This is approximately equal to the fraction of β-phase [11]. The relative amounts of monoclinic ZrO_2 (m%) and tetragonal phase were determined using the method of Garvie and Nicholson [12]. For microstructural observations, 1 μm diamond-polished specimens were thermally etched at 1500° C for 3 min and examined by SEM and optical microscopy. The grain sizes and particle size distributions were measured using a Morvideoplan image analyser. The fracture toughness (K_{Ic}) values were determined on polished specimens using the indentation technique of Evans and Charles [13]. Strength measurements were performed in three-point bending (span 14 mm) on rectangular sintered specimens of cross-section 2.2 mm × 7 mm. To determine surface strengthening, specimens were surface-ground with 320 grit SiC. The Young's modulus was calculated from the shear and the longitudinal sound velocities in the materials. These velocities were measured using the pulse-echo overlap technique.

The ionic conductivity of the 15 vol % ZrO_2–Naβ''-Al_2O_3 sample was calculated from a.c. measurements using ionically blocking silver electrodes. The impedance and the phase angles were measured using a computer-controlled low-frequency impedance analyser (HP 4192A) in the frequency range 5 Hz to 13 MHz. During measurement the sample cell was first heated to > 300° C in a vacuum and maintained at that temperature for 1 h. Data were then gathered in the maintained vacuum. The measurements were made between − 124° C and ~ 300° C.

3. Results and discussion

Acetone, methyl alcohol, butanol and ethanol have been used as milling liquids to produce ZrO_2–Naβ''-Al_2O_3 composites [1–6]. A series of studies were undertaken to identify the most suitable milling liquid to give the optimum ZrO_2 dispersion in the Naβ''-Al_2O_3 and a fine-grained homogeneous microstructure with ZrO_2 retained as tetragonal. The results for Route II are summarized in Table I. The ZrO_2 content was 8.7 vol %. Table II shows the results for the two different powder routes using the best milling liquids identified. The ZrO_2 volume fraction in this case was 15%.

Table I suggests the milling liquid influences the ZrO_2 particle size, the monoclinic ZrO_2 phase fraction and the mechanical properties. $f(\beta)$ were uninfluenced. The ZrO_2–Naβ''-Al_2O_3 composites with butanol had more agglomerates, a higher monoclinic ZrO_2 fraction and a lower density. Composites with ethanol had smaller ZrO_2 particle size, higher tetragonal ZrO_2 fraction and higher mechanical properties.

Table II shows that the two powder routes in ethanol result in almost the same physical and mechanical properties. The fracture toughness of samples milled in acetone was higher. Microstructural studies [14] showed that two ZrO_2 morphologies exist in ZrO_2–Naβ''-Al_2O_3 composites, i.e. intergranular ZrO_2 particles (or agglomomerates) located at the Naβ''-Al_2O_3 grain boundaries and fine spherical intragranular ZrO_2 particles located within the Naβ''-Al_2O_3 grains. Increased fine-grained intragranular ZrO_2 particles were detected in the microstructure of ethanol-milled samples (Fig. 1). This suggests that the ZrO_2 powder was more dispersed in ethanol and particles were trapped within the Naβ''-Al_2O_3 grains formed during sintering. These particles were fine and few were stress-induced to transform to the monoclinic phase. X-ray diffraction of the broken surfaces of test bars showed that the fraction of monoclinic phase in the

TABLE II Effect of powder route on the properties of ZrO_2–Naβ''-Al_2O_3 composites

Powder route	Milling liquid	Density (% theoretical)	Bend strength (MPa)	K_{Ic} (MPa $m^{1/2}$)	$f(\beta)$	m (%)		Grain size (μm)	
						Sintered surface	Fracture surface	β''-Al_2O_3	ZrO_2
I	Acetone	97.2 to 98.0	325 ± 54	4.2 to 4.5	0.09 to 0.10	9 to 12	92 to 96	0.84	0.71
I	Ethanol	97.0 to 97.4	330 ± 42	3.8 to 4.1	~0.03	7 to 9	–	0.81	0.73
II	Ethanol	97.2 to 97.5	336 ± 43	3.9 to 41	~0.03	9 to 11	85 to 92	0.85	0.72

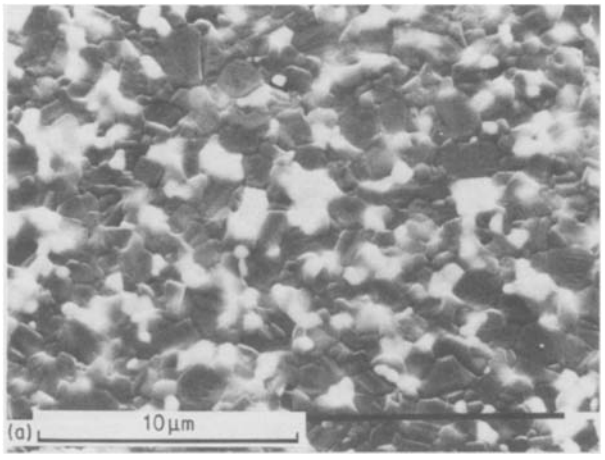

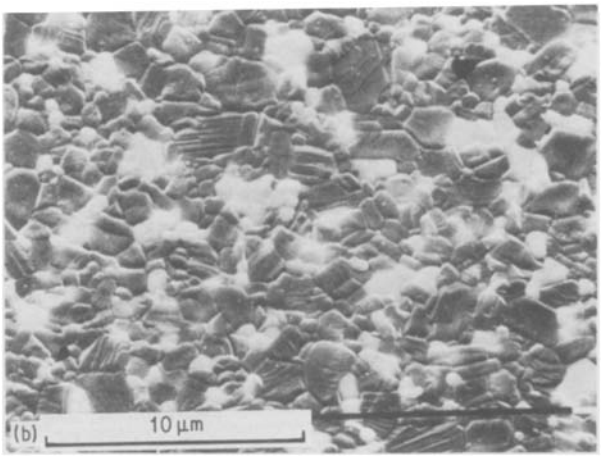

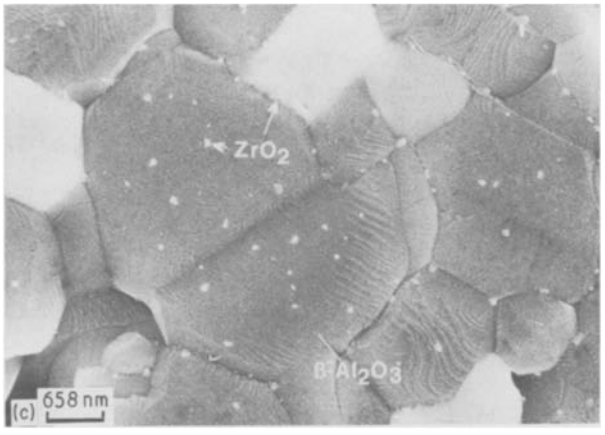

Figure 1 Microstructure of 15 vol % ZrO_2–Naβ''-Al_2O_3 composites (SEM): (a) acetone-milled sample, (b, c) ethanol-milled sample.

ethanol-milled samples was lower than with acetone (Table II).

The grain (particle) size, phase composition and mechanical properties of the ZrO_2–Naβ''-Al_2O_3 composites containing 2.5, 5, 10, 15 and 20 vol % ZrO_2 are listed in Table III.

On fast heating, the $NaAlO_2$ and Naβ/β''-Al_2O_3 eutectics form transient liquid phases, so densification is fast and the kinetics of conversion to Naβ''-Al_2O_3 rapid. It was found that the $f(\beta)$ did not increase with increasing ZrO_2. These results are contrary to those of Green [6]. The relative densities of the ZrO_2–Naβ''-Al_2O_3 composites are higher than those of pure Naβ''-Al_2O_3, suggesting that ZrO_2 improves the sinterability of Naβ''-Al_2O_3 and promotes densification. This enhanced densification could result in a higher yield of the Naβ''-Al_2O_3 phase.

Microstructural observations suggest that intergranular ZrO_2 particles limit abnormal grain growth in the Naβ''-Al_2O_3. No duplex and large grain-size microstructures were observed even after 25 min sintering. The ZrO_2 particles did not however reduce the average grain size of the Naβ''-Al_2O_3. The grain-size ratio of ZrO_2 to Naβ''-Al_2O_3 is approximately constant for a particular ZrO_2 volume fraction. Table III indicates that the ZrO_2 grain size increases with

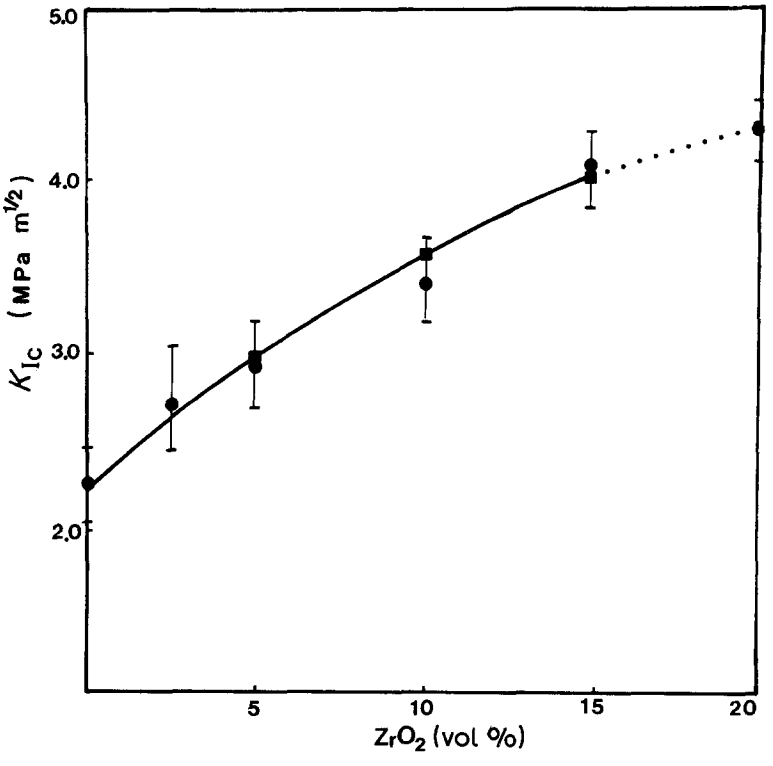

Figure 2 Fracture toughness of ZrO_2–Naβ''-Al_2O_3 against ZrO_2 content: (●) experimental data, (■) calculated values.

TABLE III Effect of ZrO_2 content on the microstructure, phase composition and properties of ZrO_2–Naβ''-Al_2O_3 composites

ZrO_2 content (vol %)	Density (% theoretical)	Bond Strength, MPa		K_{Ic} (MPa $m^{1/2}$)	Hardness, H_V	Young's modulus (MPa)	Poisson's ratio, v	$f(\beta)$	m (%)		Grain size (μm)	
		Sintered sample	Ground sample						Sintered surface	Ground surface	Naβ''-Al_2O_3	ZrO_2
0	96.0 to 97.0	223 ± 43	–	2.28 ± 0.12	1169 ± 64	185	0.273	~0.03	–	–	0.71	–
2.5	97.1 to 97.4	281 ± 52	297 ± 16	2.73 ± 0.24	1203 ± 57	187	0.274	0.06 to 0.08	13 to 17	30 to 39	0.69	0.58
5	97.2 to 98.1	312 ± 57	338 ± 61	2.96 ± 0.14	1257 ± 48	191	0.281	0.05 to 0.06	11 to 14	35 to 43	0.73	0.60
10	97.0 to 97.7	332 ± 38	340 ± 43	3.44 ± 0.13	1338 ± 51	193	0.285	0.05 to 0.07	10 to 11	15 to 21	0.84	0.69
15	97.3 to 97.7	356 ± 24	376 ± 52	4.10 ± 0.15	1383 ± 59	199	0.291	0.03 to 0.06	11 to 15	19 to 26	0.85	0.73
20	97.0 to 97.6	393 ± 53	390 ± 27	4.35 ± 0.13	1419 ± 63	–	–	0.05 to 0.07	16 to 18	28 to 34	0.67	0.79

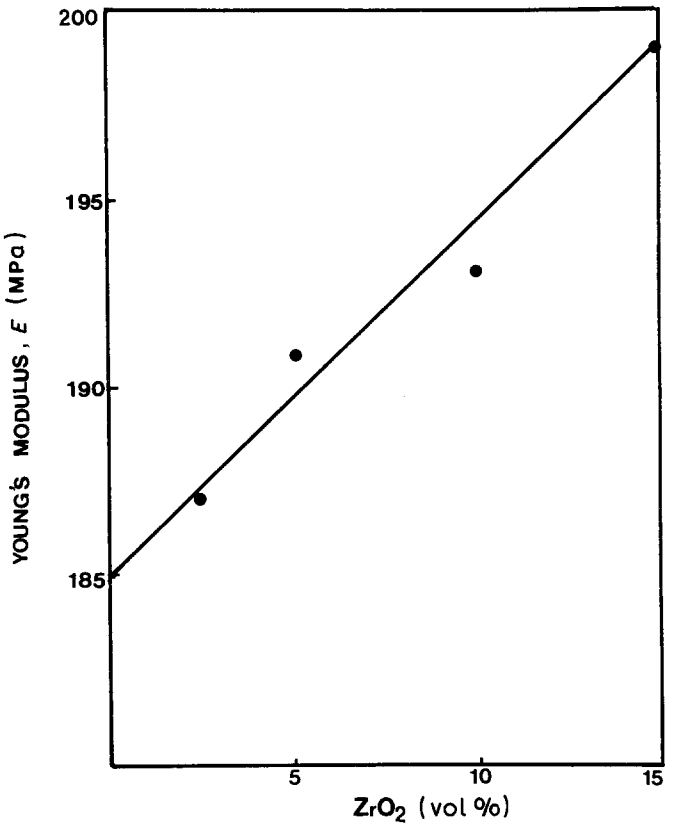

Figure 3 Young's modulus of ZrO_2–Naβ''-Al_2O_3 against ZrO_2 content.

increasing ZrO_2 volume fraction via the coalescence of the ZrO_2 particles.

The tetragonal ZrO_2 retention is high in the ZrO_2–Naβ''-Al_2O_3 composites. The level of tetragonal ZrO_2 in the composites depends on two factors, i.e. the elastic modulus of the composite and the ZrO_2 grain size. At low ZrO_2 volume fractions, the Young's modulus is low and the critical grain size small, therefore the monoclinic phase fraction is slightly higher. At higher volume fractions, there are more large ZrO_2 grains as the ZrO_2 particles coarsen. The monoclinic fraction therefore increases although the critical grain size is somewhat larger than at low ZrO_2 fractions.

The relationship between the fracture toughness and ZrO_2 content is shown in Fig. 2. In this figure, the circles plot the experimental K_{Ic} data and the solid line the calculated values. K_{Ic} increases with increasing ZrO_2 content. Young's modulus values increase with increasing ZrO_2 content (Fig. 3).

The contribution of the stress-induced transformation to the fracture toughness of a brittle material can be expressed [15] as:

$$K_{Ic} = \left(K_0^2 + \frac{2RE_cV_i(|\Delta G^c| - \Delta U_{se}f)}{(1 - \nu_c^2)}\right)^{1/2} \quad (1)$$

where K_0 is the fracture toughness of the material with no transformation phenomenon and $(|\Delta G^c| - \Delta U_{se}f)$ is the work done per unit volume to stress-induce the transformation. E_c and ν_c are the elastic modulus and Poisson's ratio of the composite, respectively, V_i is the volume fraction of the tetragonal phase and R is the depth of the transformation zone (approximately equivalent to the inclusion size). ΔG^c is the chemical free-energy change for the reaction t-$ZrO_2 \rightarrow$ m-ZrO_2, ΔU_{se} is the change in strain-energy associated with the transformation, $(1 - f)$ is the loss of strain-energy due to the loss of constraint imposed on the inclusions during crack extension. Using the experimental K_{Ic} data for the composite series containing tetragonal ZrO_2 (Table III), and obtaining K_0 values from a series containing cubic ZrO_2 exclusiyely (Table IV) and E_c and V_c values from Table III (assuming that $R = 0.7\,\mu m$), the average value of $(|\Delta G^c| - \Delta U_{se}f)$ was determined to be $185\,mJ\,m^{-3}$ for the t-ZrO_2–Naβ''-Al_2O_3 composites. The K_{Ic} for a t-ZrO_2–Naβ''-Al_2O_3 composite was then calculated from Equation 1 and these values (solid line in Fig. 2) are in good agreement with the measured results.

The results suggest that stress-induced transformation toughening is active in t-ZrO_2–Naβ''-Al_2O_3 composites. In addition to transformation toughening, the ZrO_2 inclusions could dispersion-toughen the t-ZrO_2 microstructures. The crack may avoid

TABLE IV Mechanical properties of cubic ZrO_2–Naβ''-Al_2O_3 composites

ZrO_2 content (vol %)	Density (% theoretical)	Bend strength (MPa)	K_{Ic} (MPa $m^{1/2}$)	Grain size (μm)	
				$\beta''Al_2O_3$	ZrO_2
5	97.0 to 97.7	279 ± 34	2.44 ± 0.29	–	–
10	97.2 to 97.5	282 ± 28	2.62 ± 0.35	–	–
15	97.5 to 97.8	286 ± 34	2.82 ± 14	0.79	0.86

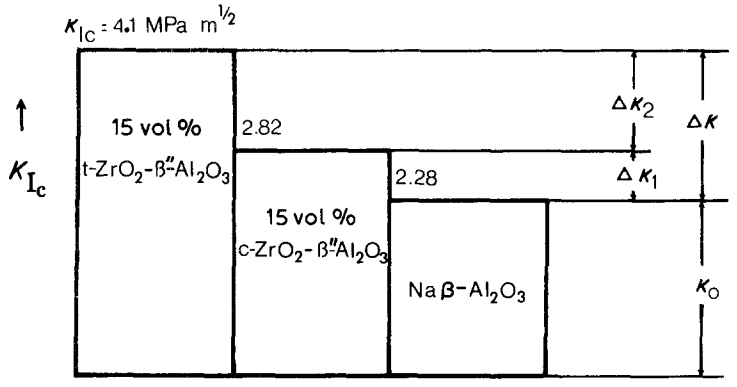

Figure 4 Contribution of dispersion toughening (ΔK_1) and transformation toughening (ΔK_2) to the toughness of ZrO_2–Naβ''-Al_2O_3 composites. (K_0 = K_{Ic} of single-phase Naβ''-Al_2O_3).

the inclusions and propagate in a zigzag path. In the 15 vol % t-ZrO_2–Naβ''-Al_2O_3 composite, K_{Ic} is 4.10 MPa $m^{1/2}$ and the increase in K_{Ic}(ΔK_{Ic}) is 1.82 MPa $m^{1/2}$ (compare single-phase Naβ''-Al_2O_3 with K_{Ic} = 2.28 MPa $m^{1/2}$). This ΔK_{Ic} can be divided into ΔK_1 and ΔK_2, where ΔK_1 is the contribution from dispersion toughening, and the ΔK_2 the contribution from transformation toughening. For the 15 vol % c-ZrO_2–Naβ''-Al_2O_3 composite (Table IV), K_{Ic} = 2.82 MPa $m^{1/2}$, i.e. ΔK_1 is 0.54 MPa $m^{1/21}$ and represents a 30% increase in K_{Ic}. If the ZrO_2 dispersion toughening is the same in both, ΔK_2 is 1.28 MPa $m^{1/2}$, i.e 70% of the total increase in K_{Ic} (Fig. 4). So, the fracture toughness of the t-ZrO_2–Naβ''-Al_2O_3 composites can be expressed as

$$K_{Ic} = K_0 + \Delta K_1 + \Delta K_2 \quad (2)$$

where ΔK_2 is the contribution of the transformation toughening, proportional to the square root of the volume fraction of ZrO_2 and ΔK_1 is proportional to the volume fraction of ZrO_2 [16]; K_0 is the fracture toughness of single-phase Naβ''-Al_2O_3. Because the ZrO_2 particles do not reduce the average grain size of the Naβ''-Al_2O_3, it is assumed that the grain-size factor does not contribute to the increased fracture toughness.

The dependence of bend strength on ZrO_2 content is shown in Fig. 5. Line 1 is based on the measured values of the sintered samples. Line 2 is the calculated value using the relation $\sigma_1 = (K_1/K_0)\sigma_0$ assuming no change in flaw size. σ_0 and K_0 are the strength and fracture toughness of single-phase Naβ''-Al_2O_3 and σ_1 and K_1 are the strength and fracture toughness of the composite, respectively.

The bend strength (Line 1) increased with increasing ZrO_2 volume fraction. These results are different from those of Binner and Stevens [4]. No maximum was seen in the strength–ZrO_2 content curve up to 20 vol % ZrO_2. It is believed that 85 to 90% of the tetragonal phase was retained at the higher ZrO_2 contents and the bend strength increased accordingly.

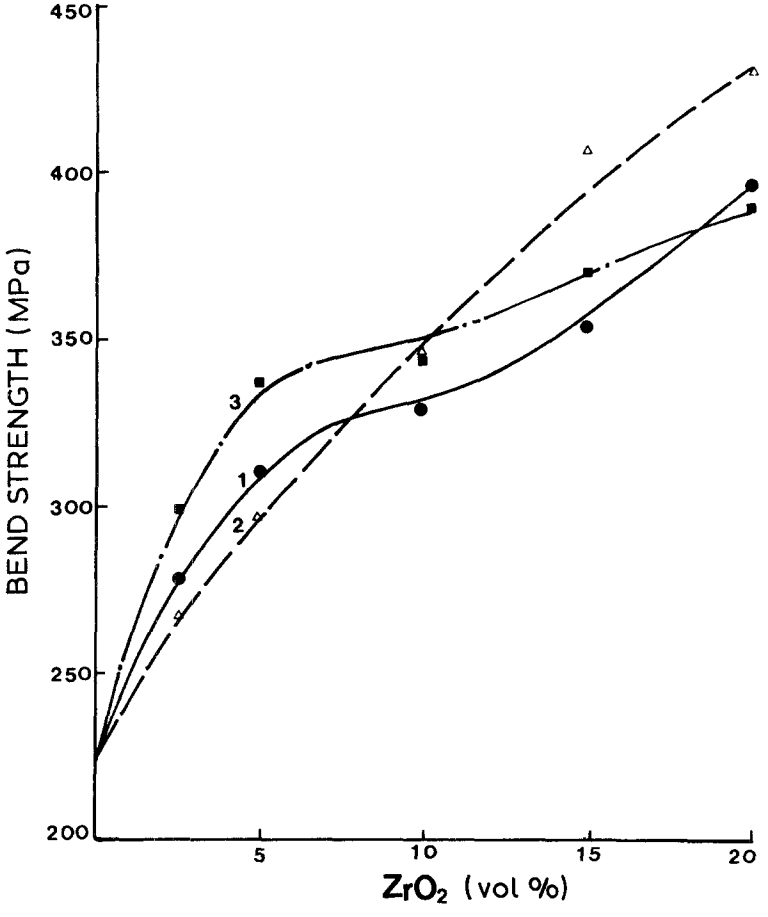

Figure 5 Bend strength of ZrO_2–β''-Al_2O_3 against ZrO_2 content: (●) sintered samples, (■) ground samples, (△) predicted strength.

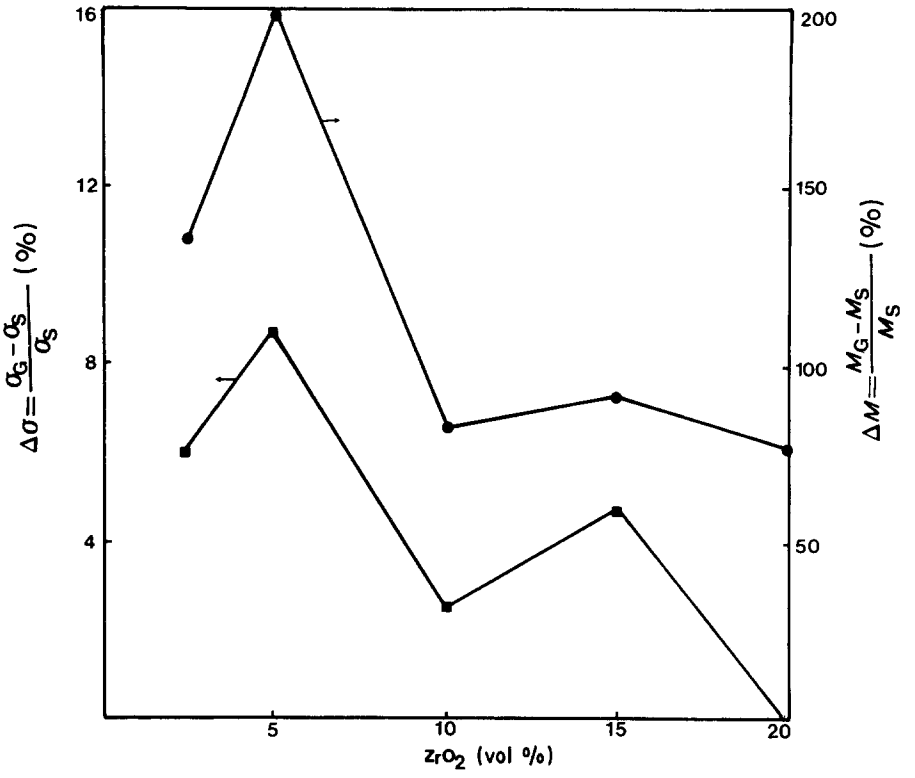

Figure 6 Increase in strength and monoclinic ZrO_2 fraction against ZrO_2 content. σ_G: the strength of ground sample; σ_S: the strength of sintered sample; M_G: the monoclinic ZrO_2 fraction of ground sample; M_S: the monoclinic ZrO_2 fraction of sintered sample.

The calculated values of strength were in good agreement with the experimental values. The bend strength exhibited a concomitant increase with K_{Ic}. These results are different from those of Green and Metcalf [5, 6], who found that the predicted strength from the K_{Ic} value was much lower than the measured value for either composite. However, at high ZrO_2 contents, the measured values of strength were lower than the predicted values, possibly due to an increase of the monoclinic ZrO_2 fraction and the generation of microcracks.

Surface strengthening has been used to improve the strength of transformation-toughened materials [17, 18]. In transformation-toughened ZrO_2 ceramics, grinding causes the surface tetragonal ZrO_2 to transform to monoclinic and the associated expansion places the surface in compression and so strengthens the ceramic.

The bend strength of ground samples is also plotted against ZrO_2 content in Fig. 5 (Line 3). The increase in strength is greater at lower ZrO_2 contents. This is due to the reduced elastic modulus of the composite at low ZrO_2 contents, which reduces the "constraint" on the surface ZrO_2 particles and allows their transformation to proceed. As shown in Fig. 5, the increase in strength of ground samples parallels the increase of monoclinic ZrO_2 fraction. The hardness of the composite decreases with decreasing ZrO_2 content, so the depth of the compressive transformation layer is increased under certain grinding conditions. The low ZrO_2 content composites attain the compressive layer thickness necessary for strengthening.

It is interesting to note that the maximum increase in strength occurs at 4 vol % ZrO_2 (Fig. 6). The maximum strength occurred at ~4 vol % ZrO_2 in the work of Binner and Stevens [4] in which the bars for strength measurements were cut from pellets and the faces ground on a ~35 μm diamond wheel. It is assumed that the data reported are the strengths after surface strengthening.

The critical grain sizes of the ZrO_2 in the ZrO_2–Naβ''-Al_2O_3 composites are listed in Table V. The critical grain size was determined by comparing the monoclinic-phase ZrO_2 fraction with the grain size distribution and assuming that the tetragonal grains were smaller than the monoclinic ZrO_2 grains. The results indicate that the critical grain size increases with increasing ZrO_2 volume fraction. The critical grain size for the present ZrO_2–Naβ''-Al_2O_3 composite containing ~15 vol % ZrO_2 is ~1 μm, a result similar to that of Viswanathan *et al.* [2].

Turning to the electrical measurements, a polycrystalline fast ionic ceramic can be modelled by a simple equivalent circuit considering the grains (bulk), the grain boundaries and the electrode interfaces. Fig. 7a shows the equivalent circuit originally developed by Bauerle [19]. To separate the bulk, grain-boundary and electrode effects, the complex plane impedance and admittance are analysed. Fig. 7b shows the complex-plane impedance plots and Fig. 7c

TABLE V Critical grain size for the retention of t-ZrO_2 in ZrO_2–Naβ''-Al_2O_3 composites

ZrO_2 content (vol %)	Sintering temperature (°C)	Sintering time (min)	Critical grain size (μm)
2.5	1620	10	0.86
5	1620	10	0.98
10	1620	10	1.02
10	1620	60	1.09
10	1620	120	1.03
10	1620	180	1.05
15	1620	10	0.92
15	1620	60	1.07
15	1620	120	1.04
15	1620	180	1.12

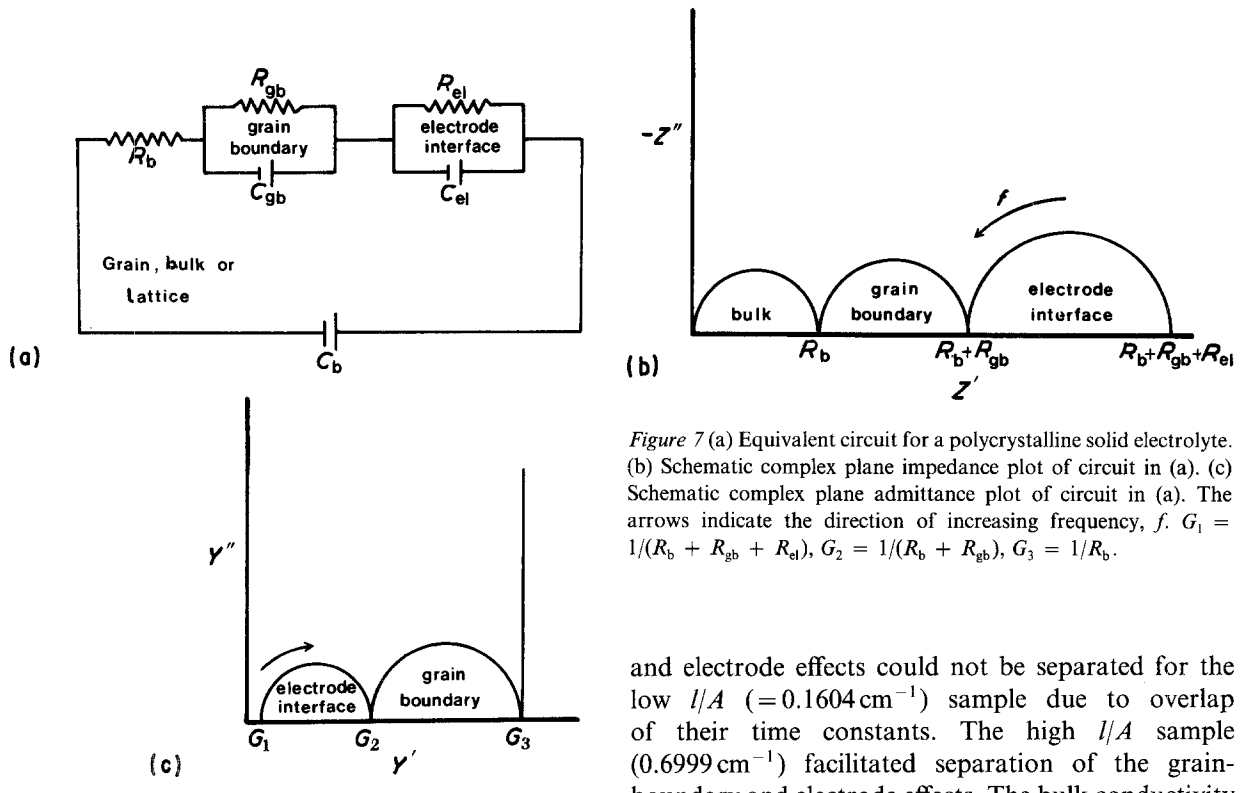

Figure 7 (a) Equivalent circuit for a polycrystalline solid electrolyte. (b) Schematic complex plane impedance plot of circuit in (a). (c) Schematic complex plane admittance plot of circuit in (a). The arrows indicate the direction of increasing frequency, f. $G_1 = 1/(R_b + R_{gb} + R_{el})$, $G_2 = 1/(R_b + R_{gb})$, $G_3 = 1/R_b$.

shows the complex-plane admittance plot for the circuit shown in Fig. 7a. The complex-plane impedance and admittance plots for 15 vol % ZrO_2–Naβ''-Al_2O_3 at $-75°$ C are shown in Fig. 8. These figures show three distinctly different regions associated with the grains (bulk), grain boundaries and the electrode interface effects. Measurements were conducted between $-124°$ C and $\sim 300°$ C using two samples of different dimensions (l/A ratios where l = thickness and A = cross-sectional area). The grain-boundary and electrode effects could not be separated for the low l/A ($=0.1604\,cm^{-1}$) sample due to overlap of their time constants. The high l/A sample ($0.6999\,cm^{-1}$) facilitated separation of the grain-boundary and electrode effects. The bulk conductivity was calculated from the impedance plots and the total conductivity from the admittance plots. At 300° C, the total resistivity (grains + grain boundaries) was $\sim 9\,\Omega$cm. At the same temperature, the literature-reported [20, 21] single crystal resistivity varies between 1.0 and $2.5\,\Omega$cm. The 15 vol % ZrO_2 dispersed Naβ''-Al_2O_3 composite has electrical properties satisfactory for practical applications.

Fig. 9 is an Arrhenius plot of $\log(\sigma T)$ against $10^4/T$ for the bulk and total conductivities (σ = conductivity).

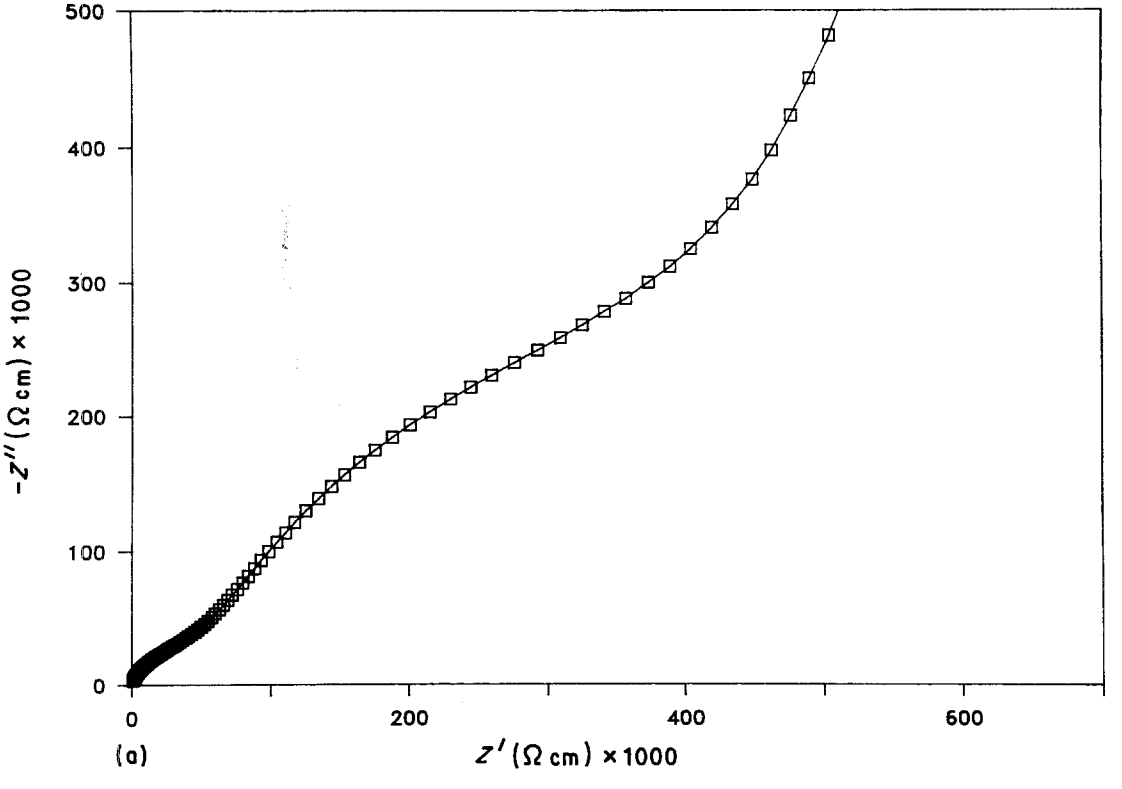

Figure 8 (a) Complex plane impedance. (b) Complex plane admittance plots for 15 vol % ZrO_2–Naβ''-Al_2O_3 at $-75°$ C. (B is the imaginary part of the admittance).

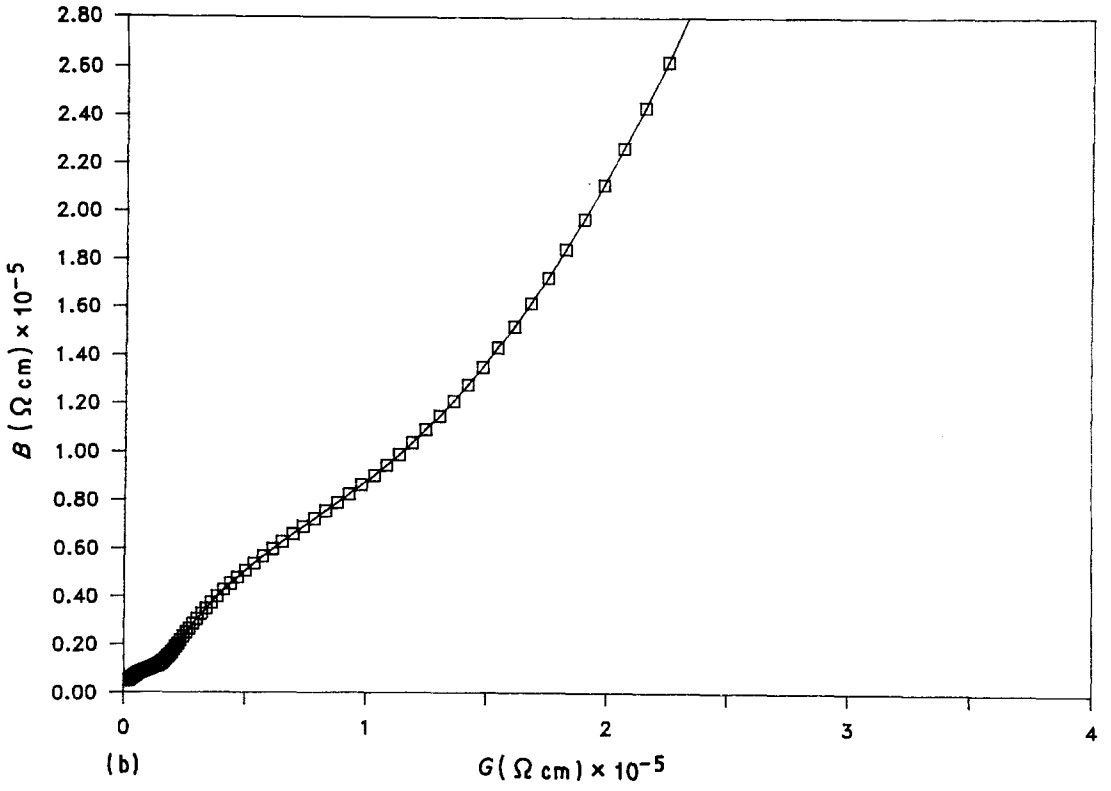

Figure 8 Continued

The activation energy of the bulk and total conductivity processes are 0.30 and 0.32 eV, respectively.

Accepted resistivity values for a good polycrystalline Naβ''-Al_2O_3 ceramic are $\sim 5\,\Omega$cm. The present value of $9\,\Omega$cm indicates the role of the grain boundary in increasing the ceramic resistivity. This could be associated with the volume fraction of the resistive ZrO_2.

4. Conclusions

As a result of the investigations here reported, the following conclusions can be made:

1. The fracture toughness (K_{Ic}) and Young's modulus (E) increase with increasing ZrO_2 content in ZrO_2–Naβ''-Al_2O_3 composites. Stress-induced transformation toughening is the predominant toughening

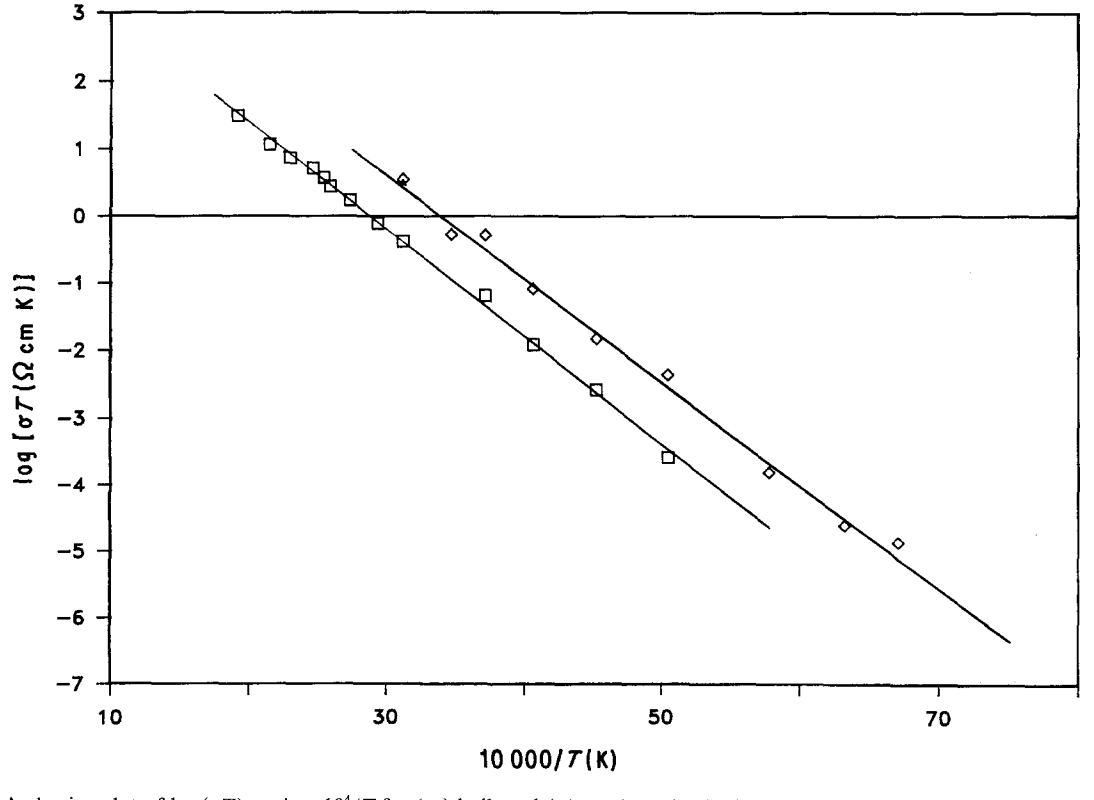

Figure 9 Arrhenius plot of $\log(\sigma T)$ against $10^4/T$ for (◇) bulk and (□) total conductivities.

mechanism. Dispersion toughening also contributes to the increase of K_{Ic}.

2. The bend strength increases with increasing ZrO_2 content up to 20 vol % ZrO_2.

3. Surface strengthening by grinding is an effective way to improve the strength of ZrO_2–Naβ''-Al_2O_3 composites. The increase of strength is higher for lower ZrO_2 contents.

4. The critical grain size for retention of tetragonal ZrO_2 increases with increasing ZrO_2 content.

5. The specific resistivity of the 15 vol % ZrO_2–Naβ''-Al_2O_3 composites was 9 Ω cm at 300° C, the activation energies of the bulk and total conductivity processes being 0.3 and 0.32 eV, respectively.

Acknowledgements

The authors are grateful to T. Troczynski for his helpful suggestions, D. Misale, S. Kamenschik and A. Gryzmek for technical assistance, Dr N. D. Patel for measurement of Young's modulus and Arthur J. Stockman for helping with computer-related problems.

References

1. F. F. LANGE, B. I. DAVIES and D. O. RALEIGH, *J. Amer. Ceram. Soc.* **66** (3) (1983) C50-52.
2. L. VISWANATHAN, Y. IKUMA and A. V. VIRKAR, *J. Mater. Sci.* **198** (1983) 109.
3. J. D. BINNER, R. STEVENS and S. R. TAN, *Adv. Ceram.* **12** (1983) 428.
4. J. G. BINNER and R. STEVENS, *J. Mater. Sci.* **20** (1985) 3119.
5. D. J. GREEN and M. G. METCALF, *Amer. Ceram. Soc. Bull.* **63** (1984) 803.
6. D. J. GREEN, *J. Mater. Sci.* **20** (1985) 2639.
7. A. V. VIKAR, *ibid.* **16** (1981) 1142.
8. L. A. FELDMAN, *ibid.* **17** (1982) 517.
9. P. S. NICHOLSON, M. NAGAI, K. YAMASHITA, M. SANGER and M. F. BELL, *Solid State Ionics*, **15** (1985) 317.
10. J. T. KUMMER, *Prog. Solid State Chem.* **7** (1972) 141.
11. A. PEKARSKY and P. S. NICHOLSON, *Mater. Res. Bull.* **15** (1980) 1517.
12. R. C. GARVIE and P. S. NICHOLSON, *J. Amer. Ceram. Soc.* **55**(6) (1972) 303.
13. A. G. EVANS and E. A. CHARLES, *ibid.* **59**(7-8) (1976) 371.
14. YIN SHENG and P. S. NICHOLSON, *J. Mater. Sci.* **23** (1988) 982.
15. F. F. LANGE, *ibid.* **17** (1982) 235.
16. J. C. M. LI and S. C. SANDAY, *Acta Metall.* **34** (1986) 537.
17. R. T. PASCOE and R. C. GARVIE, in "Ceramic Microstructures '76" edited by R. M. Fulrath and J. A. Pask (Westview, Boulder, Colorado, 1977) pp. 774–784.
18. N. CLAUSSEN, *J. Amer. Ceram. Soc.* **61** (1-2) (1978) 85.
19. J. E. BAUERLE, *J. Phys. Chem. Solids* **30** (1969) 2657.
20. G. C. FARRINGTON and J. L. BRIANT, "Fast Ion Transport in Solids" edited by P. Vashista, J. N. Mundy and G. K. Shenoy (North-Holland, Amsterdam, 1979) p. 395.
21. J. B. BATES, in "Fast Ion Transport in Solids" edited by P. Vashista, J. N. Mundy and G. K. Shenoy (North-Holland, Amsterdam, 1979) p. 261.

Received 28 April
and accepted 6 July 1987